HHS Public Access

Author manuscript

Nanotechnology. Author manuscript; available in PMC 2015 July 30.

Published in final edited form as:

Nanotechnology. 2014 February 7; 25(5): 055101. doi:10.1088/0957-4484/25/5/055101.

Enhanced blood-brain barrier transmigration using a novel Transferrin-embedded fluorescent magnetoliposome nanoformulation

Hong Ding[1,2], **Vidya Sagar**[1,2], **Marisela Agudelo**[2], **Sudheesh Pilakka-Kanthikeel**[1,2], **Venkata Subba Rao Atluri**[2], **Andrea Raymond**[2], **Samikkannu Thangavel**[2], and **Madhavan P. Nair**[1,2,*]

[1]Center for Personalized Nanomedicine, Department of Immunology, Herbert Wertheim College of Medicine, Florida International University, Miami, Florida 33199, USA

[2]Institute of NeuroImmune Pharmacology, Department of Immunology, Herbert Wertheim College of Medicine, Florida International University, Miami, Florida 33199, USA

Abstract

Blood-brain barrier (BBB) is considered as the primary impediment barrier for most of drugs. Delivering therapeutic agents to brain is still a big challenge by now. In our study, a dual mechanism, receptor mediation combining with external non-invasive magnetic force, was incorporated together into ferrous magnet-based liposome for BBB transmigration enhancement. The homogenous magnetic nanoparticles (MNPs) with size of ~ 10 nm were synthesized and confirmed by TEM and XRD respectively. The classical magnetism assay showed presence of characteristic superparamagnetic property. These MNPs encapsulated in PEGylated fluorescent liposomes as magneto liposomes (ML) showed mono-dispersion ~ 130±10 nm diameter by dynamic laser scattering (DLS) using lipid-extrusion technique. Remarkably, this magnetite encapsulation efficiency of nearly 60% was achieved. And the luminescence and hydrodynamic size of ML was stable for over two months under 4 degree. Additionally, the integrity of ML structure remained unaffected through 120 rounds circulation mimicking human blood fluid. After biocompatibility confirmation by cytotoxicity evaluation, these fluorescent ML was further embedded with Transferrin and applied to *in vitro* BBB transmigration study in presence or absence of external magnetic force. Comparing with only by magnetic force- or Transferrin receptor-mediated transportation, their synergy resulted in 50–100% increased transmigration without affecting the BBB integrity. Consequently, confocal microscopy and iron concentration in BBB-composed cells further confirmed the higher cellular uptake of ML particles due to synergic effect. Thus, our multi-functional liposomal magnetic nanocarriers possess great potential in particles transmigration across BBB and may have bright future in drug delivery to brain.

Keywords

Magnetic nanoparticles (MNPs); Magneto liposome (ML); Blood-brain barrier (BBB); Fluorescence; Transferrin; transmigration

*Corresponding Authors: Madhavan P. Nair. Tel: 305-348-1493, Fax: 305-348-1109. nairm@fiu.edu.

1. Introduction

The blood–brain barrier (BBB) separates central nervous system (CNS) from peripheral circulation (blood). It mainly consists of brain microvascular endothelial cells (BMECs), and tightly connected with primarily neuronal pericytes and perivascular astrocytes. [1–3] Together with this distinct structure, the enzymes and endocytic activity of BMECs regulate the transport of both exogenous and endogenous materials to brain in a very selective and specific manner. [4–7] Only molecules essential for brain function such as certain amino acids, monocarboxylic acids, amines, sugars, purine bases, oxygen and carbon dioxide, certain neurotransmitters, and small lipophilic molecules up to molecular weight of 400–500 Dalton can diffuse across the BBB.[6; 8] Nevertheless, permeability of all these selective molecules provides very little or no benefit for most diseases within brain. Meanwhile, extensive presence of multi-drug efflux pump transporters on the membrane of BMECs further prevents entry of almost all drugs across BBB and staying into brain. [5, 6]

In general, there are three transport mechanisms in the BBB: passive-, receptors mediated-, and vesicular-carriers. [9] After several unsuccessful trials including passive drug delivery (e.g. hydrophobic modification, prodrug design, etc.) and active drug delivery (e.g. target ligand conjugation), nanotechnology-based approaches appears to have significant advantages on BBB transmigration due to the particle size and surface modifications. The use of nanotechnology research to develop novel nanoformulations is an innovative area in CNS pharmacology. Recently, theranostic (therapy + diagnosis) nanomedicine has drawn considerable attention for CNS treatment due to its integrating target, imaging and therapy in one system. [10–12] In current clinic, magnetic resonance imaging (MRI) has been a widely applied image modality especial for soft tissue.[13–15] Colloidal iron oxide nanoparticles such as superpara-magnetic iron oxide (SPOI) and ultrasmall superparamagnetic iron oxide (USPIO) have been used as MRI contrast radio-labeled agents or and target drug delivery for theranostics. [16–19]

Among the existing nanocarriers such as polymeric nanoparticles, dendrimers, solid-lipid nanoparticles and liposomes etc, iron oxide (Fe_3O_4) based magnetic nanoparticles (MNPs) showed advantage as theranostic carriers for CNS diseases treatment. It can be employed as MRI guided drug delivery.[16; 17; 20; 21] In Gao’s group, hydrophilic poly(ethylene glycol) (PEG) layer coated Fe_3O_4 nanoparticles were covalently bonded with lactoferrin (Lf) and tested for BBB transmigration. [22] This strategy had its major drawback due to the strong shielding effect from thick PEG corona, which may prevent the interaction between the bonded ligand and its BBB receptor. [23] Saiyed et al. encapsulated MNPs with liposomes significantly improved the BBB transmigration while the mechanism is not very clear. And the crossing efficiency still needs to be improved.[24]

Liposomes have been widely applied as drug carriers in preclinic and clinic. [25–27] Several therapeutic agents such as small molecules, [28] proteins, [26] peptides, [29] DNA, [30] and RNA, [31] have been tethered in liposomes. Incorporation of MNPs with liposomes provides several advantages: i) drugs bounded on MNPs can be maintained into the liposomal inner space (or the phospholipid bilayers) with higher loading efficiency; ii) liposomes can protect the MNPs bound drugs from the enzymatic degradations from

peripheral circulation (blood) resulting in longer circulation period and higher bioavailability; iii) the moving direction of MNPs is controllable by external magnetic force for the target delivery; iv) it is possible to couple protein (e.g. receptor-specific ligand) on the liposomal bilayer for drug delivery or achieving specific cellular recognition. Therefore, multiple functional magnetized-liposomal nanocarriers may provide a highly effective nanoformulation platform for drugs delivery. However, few studies on this synergetic transmigration mechanism of receptor mediation and non-invasive magnetic force have been explored.

It is well-known that Transferrin receptor is a BBB specific transporter that allows Transferrin to attach and BBB membrane across. [32–34] Such receptor-mediated approach may provide a promising avenue for CNS targeting. In the current work, Transferrin was embedded on the fluorescence labeled magnetized liposome and used for transmigration across *in vitro* BBB model. Herein, for the first time, we reported the incorporation of dual transport mechanism in one nanocarrier which combined the external magnetic force and receptor-mediation. Studies on transmigrated nanocarriers from apical to basolateral layers in *in vitro* BBB model, permeability index i.e. transendothelial electrical resistance (TEER) of BBB, cellular ferrous concentration in BBB-composed cells were performed. The results suggested that this dual mechanism carrier may be applied as a high efficient, real-time theranostic platform for targeted-delivery to brain. We believe that this novel approach with high biocompatibility may open a bright avenue for CNS drug delivery.

2. Materials and Experimental

2.1. Materials

Iron (III) chloride ($FeCl_3$, Cat#: 451649), sodium sulfite (Na_2SO_3, Cat#: 71989), hydrochloric acid (HCl, Cat#: 320331), Ammonium thiocyanate (NH_4, SCN, Cat#: 431354), ammonium persulfate ($(NH_4)_2S_2O_8$, Cat#: 248614), ammonium hydroxide solution ($NH_3.H_2O$, Cat#: 320145), and Transferrin (Cat#: T4132) were purchased from Sigma-Aldrich (St. Louis, MO, USA). Unless notified, water used for all reactions was HPLC grade. Egg phosphatidylcholine (EPC, Cat#: 830071P), 1,2-distearoyl-sn-glycero-3-phosphoethnolamine-N-[methyoxy(polyethylene glycol)-2000] ($mPEG_{2000}$-DSPE, Cat#: 880128P), 1,2-distearoyl-sn-glycero-3-phosphoethnolamine-N-carboxylfluorescein (CFPE, Cat#: 810332), and cholesterol (Chol, Cat#: 700000P) were obtained from Avanti Polar Lipids (Alabaster, AL, USA). The tetrazolium compound [3-(4, 5-dimethyl thiazol-2-yl)-5-(3-carboxy-methoxyphenyl)-2-(4-sulfophenyl)-2H-tetrazolium, inner salt (MTS, Cat#: G3580) was purchased from Promega Corporation (Fitchburg, WI, USA). Human brain endothelial cell (HMBVEC, Cat#: 1000), human brain astrocytes (HA, Cat#: 1800) and their culture medium (Cat#: 1001 and 1801 respectively) were brought from ScienCell Research Laboratories (Carlsbad, CA, USA).

2.2. Synthesis of ultrasmall MNPs

The ultrasmall Fe_3O_4 based MNPs were synthesized by co-precipitation method proposed by Dr. Sun with minor modification. [35] All glassware was cleaned overnight by aqua regia before used. Briefly, 3 ml of $FeCl_3$ (0.487 g dissolved in 2 mol/L HCl) was added to 10.33

ml of H_2O and 2 ml of Na_2SO_3 (0.126 g in 2 ml of water) was added into the former solution drop wise within one minute under stirring. After the color of reaction solution was changed from yellow to red-light yellow, this solution was poured into 80ml of ammonium hydroxide solution (0.85 mol/L) under vigorous stirring. A black precipitate was quickly formed, which was allowed to crystallize further for another half hour under continuously stirring. After washing, the pH value of the suspension was 7.5. In order to form stable MNPs, pH was adjusted from 7.5 to 3.0 and temperature was raised to 90°C for five minutes and then 100°C for one hour. A change in color of dispersion from black to reddish-brown suggested the successfully MNPs formation with three times washing separated by decantation method.

2.3. Formulation of PEGylated magneto-liposome (ML) and Transferrin (Tf) embedding

Preparation of PEGylated liposomes and encapsulation of MNPs in its inner space was achieved by extrusion method. [36] 7:2:0.5 molar ratios of EPC, Cholesterol, and mPEG2000-DSPE was thoroughly mixed in chloroform and evaporated under vacuum. 1.0 mg of ultrasmall MNPs was added onto the resultant thin lipid film for rehydration. PEGylated liposomal vesicles containing MNPs was formed by handheld extruder (Avanti Polar Lipids, Inc.) containing polycarbonate membrane filter of different pore size (400nm/200nm/100nm, respectively). Prior to extrusions, the mixture was warmed by using a hot plate at a temperature above the transition temperature of lipids. The resulting unilamellar ML nano-vehicles with homogenous size were separated from unloaded MNPs by centrifugation at 1,000 rpm for two minutes. The purified MLs were stored at 4°C for further usage. Fluorescent labeling was achieved by adding 0.8% of CFPE relative to the total lipids into the initial liposome formulation mixture.

Transferrin embedding was achieved by mixing 0.5mg fresh Transferrin into 200μL of prepared magnetic-liposome at 37°C for ~30 min. [37]

2.4. Characterization of MNPs and their liposomal formulation

2.4.1. X-ray diffraction (XRD) and transmission electron microscopy (TEM) analysis—Structural conformation of MNPs was determined by Shimadzu XRD-7000 diffractometer (Shimazdu, Tokyo, Japan). TEM of MNPs/MLs was performed with the Phillips CM-200 200 kV transmission electron microscope operated at 80 kV. In brief, one drop of MNPs or magneto-liposomes was spread on carbon support film on 400 mesh Cu grids (Type B, Ted Pella, Inc., USA). For better contrast during TEM imaging, samples on grid were negatively stained with phosphotungstic acid (2.0% w/v; pH 6.4) and dried at room temperature.

2.4.2. Particle size and zeta potential—The hydrodynamic radius, size distribution, and surface charge measurement of MNPs/MLs were carried out at 25°C in dynamic laser scattering (DLS) (90 Plus Particles Size Analyzer, Brookhaven Instrument Corp., USA).

2.4.3. Superparamagnetism measurement—The measurement of superparamagnetism was carried out by classical vibrating sample magnetometer (Model

4HF VSM, USA). The magnetic hysteresis loops of the Fe_3O_4 particles were measured between +1200 to − 1200 Oersted (Oe) at room temperature.

2.4.4. Determination of encapsulation efficiency (EE)—The encapsulation efficiency value designated the percentage of MNPs loaded in liposomes and was estimated by the ratio between the iron concentration in ML before and after encapsulation. It was calculated as: EE (%) = (Iron concentration in magneto-liposome)/(Iron concentration fed) ×100%

2.4.5. Measurement of encapsulated MNPs in liposome—Ammonium thiocyanate-based photometric assay was used to determine the amount of encapsulated Fe_3O_4. ML formulation was mixed with Triton X-100 (1%, v/v) in a ratio of 1:1.5 causing de-encapsulation of MNPs. One volume concentrated HCl (37%) was added to this mixture and incubated at 60°C for 4 hours. The suspension was centrifuged at 12,000 g for 10 minutes and supernatant was collected for quantification of iron concentration. Equal ratio of supernatant and 1% ammonium persulfate solution was mixed with one volume 0.1 M Ammonium thiocyanate and incubated at RT for 5 minutes. The absorption of resulting red iron-thiocyanate was measured at 490 nm by a microplate reader (Synergy HT, Multi-mode microplate reader, BioTek Instrument, Inc., Winooski, Vermont, USA). A standard curve was prepared with known concentrations of Fe_3O_4 in H_2O.

2.4.6. Validation of Transferrin (Tf) embedding—Embedding of Transferrin in the periphery of ML was determined spectrophotometrically with UV-visible spectrophotometer (Varian, USA). Presence of Transferrin-specific absorbance was measured by scanning wavelength range from 250–400nm.

2.5 Measurement of colloidal- and fluorescent-integrity of MLs

The hydrodynamic size of MLs was determined by DLS (90 Plus Particles Size Analyzer, Brookhaven Instrument Corp., USA). The nanocarriers were stored at 4°C and durability of their structural-integrity was evaluated by measuring the size for up to 28 days. Further, their stability in blood fluid was assessed by measuring the size in an *in vitro* closed circulatory system at 37°C for up to 28 hrs. This closed circulation system was set up using a bidirectional, self-priming peristaltic pump (Mini Pump Peristaltic Pump Variable Flow C-2 Lab Pump, Fisher Scientific). The nanoformulation was allowed to circulate in a 0.8 mm capillary for 120 times at a flow rate of 1ml/min. The circulating medium was prepared with 5% dextran-500 (Cat #: 50-247-495, Thermo Fisher Scientific, Boston, US) in PBS which made a viscosity equivalent to that of blood (4.5 centipoise). Samples were collected after 10, 30, 60, and 120 circulations and subjected to the size analysis by DLS.

The fluorescent-integrity of MLs was determined by measuring the fluorescent intensity of associated CFPE at wavelength 485/20nm-528/20 nm (Ex/Em) by microplate reader (Synergy HT, Multi-mode microplate reader, BioTek Instrument, Inc., Winooski, Vermont, USA).

2.6. *In vitro* blood-brain barrier (BBB) model

The primary human brain microvascular endothelial cells (HBMEC) and human astrocyte (HA) cells were cultivated as per provider's recommendations. The BBB model was established as described earlier by Gandhi et al. [38] In brief, the *in vitro* BBB model was developed in a bi-compartmental transwell culture plate (Product # 3415, corning life sciences, Mexico). The upper chamber of this plate was separated from the lower one by a 10 μm of thick polycarbonate membrane possessing 3.0 μm pores. In a sterile 24-well cell culture plate with pore density of 2×10^6 pores/cm^2 and cell growth area of 0.33 cm$^2 2\times10^5$ HBMEC and HA were grown to confluency on the upper chamber and underside of lower chamber respectively. Intactness of in BBB was determined by measuring the transendothelial electrical resistance (TEER) using Millicell ERS microelectrodes (Millipore). A mean TEER value of ~200 ohms/cm^2 cell culture insert was considered as the formation of the BBB.

2.7. Transmigration of fluorescent MLs across *in vitro* BBB model

Transmigration study of ML nanoformulations was conducted on the 5th–6th day of the BBB culture after the memberane integrity was established as confirmed by TEER measurement. Equal quantity of Transferrin embedded and/or non-embedded fluorescent MLs were added to the apical chamber and incubated at 37°C in the presence or absence of a magnetic force of 0.08 Tesla placed externally below the trans-well's basolateral chamber. Samples were collected from both the chambers at determined time points and fluorescent intensities were measured at wavelength 485/20nm-528/20 nm (Ex/Em) by microplate reader (Synergy HT, Multi-mode microplate reader, BioTek Instrument, Inc., Winooski, Vermont, USA).

The relative apparent permeability coefficient was calculated from the equation as: Relative Papp = (Fluorescent intensity in basal chamber)/(Fluorescent intensity in apical chamber) × 100

Where Papp: apparent permeability

2.8. Cell uptake evaluation

2.8.1. Confocal microscopy—HBMEC and HA cells were seeded on cover-slip in six-well plates with a concentration of 1×10^6 cells. After 24 hrs, cells were treated with equal quantity of Transferrin embedded and/or non-embedded fluorescent MLs in the presence and/or absence of external magnetic force for 4 hours. Cells were rinsed three times with PBS and fixed with 4% Paraformaldehyde in PBS for 30 min at room temperature. Cover-slips were mounted on the slides with Prolong®Gold antifade reagent (Invitrogen) and fluorescent intensity were detected using TCS SP2 Confocal Laser Scanning Microscope (Leica Microsystems, Germany). Confocal images were obtained at 488nm (100%) illusion of an argon-ion laser using 60X oil immersion objectives with high numeric aperture and 2.5X confocal electronic zoom settings.

2.8.2. Cellular iron content measurement—After 2 hours treatment with equal quantity of Transferrin embedded and/or non-embedded fluorescent MLs in the presence and/or absence of external magnetic force, cells from each treatment groups were

centrifuged at 4,500g for 5 minutes. Cell pellets were subjected for quantification of uptake iron content in each treatment group by ammonium thiocyanate-based photometric assay in similar to that described for liposomes in section 2.4.5. [39; 40]

2.9. Cytotoxicity assay

Cytotoxicity was assessed by MTS cell viability assay using CellTiter 96®Aqueous one solution cell proliferation assay kit (Catalog # G 3580, Promega, USA).[41] HBMEC and HA cells were seeded in 96-well tissue plates at a density of 5×10^3 cells/well. After 24 hours, culture medium was replaced with 100 μl fresh media containing different concentrations of Fe_3O_4 (from 0.02–0.5 mg/mL^{-1}). 20 μL of MTS solution was added into each well 24 and 48 hour post-treatment and incubated at 37°C for 2 hours. Absorbance was recorded at 490 nm by microplate reader (Synergy HT, Multi-mode microplate reader, BioTek Instrument, Inc., Winooski, Vermont, USA)

2.10. Statistical analysis

All experiments were performed at least three times in duplicates and values were expressed as means ± standard derivation (SD). Unpaired student's t-test was performed and P values ≤ 0.05 were regarded as the significance.

3. Results and Discussion

Magnetite (Fe_3O_4) is the most commonly used magnetic nanoparticles in the field of biomedicine, mainly due to its biocompatibility and specific surface properties. In the view of nanotechnology, MNPs with different sizes, ranging from a few up to tens of nanometers, have been investigated for disease diagnosis and target drug delivery. Generally, drugs are either directly immobilized on the MNPs surface or tethered via coating of organic/inorganic polymer layer such as PEG. In either case, free drugs are exposed to external environment and possess threat of rapid decomposition due to metabolism (enzymztic mainly) of peripheral circulation (blood) before it could reach to target. Thus, an effort to protect drugs from exterior degradation must be considered for advancement of MNPs-based drug delivery. Recently, a hybridization strategy where MNPs is encapsulated in liposomes termed magneto-liposome (ML), has emerged as a possible solution. However, potential application of ML-based drug delivery across blood-brain barrier (BBB), in CNS, is very limited. In the wake of CNS sophisticacy, an ideal drug delivery carrier should incorporate maximum drug bioavailability with minimum waste constituent. One way this could be achieved is by increasing the encapsulation potential of liposomes with no affect on overall ML size. Higher loading density of MNPs in liposomes would require synthesis of smallest particles which suitable for the targetting and drug-bioavailablity. Particles of >10 nm can sustain in the the systemic circulation; however, that of lesser size lost due to permeability of vascular endothelium and prohibits drugs to reach target-site.

There are several methods to synthesize Fe_3O_4 nanoparticles such as co-precipitation, microemulsion, high temperature decomposition, oxidation of magnetite, etc.[24; 35; 39; 42] Co-precipitation is regarded as one of the most efficient, circumstance friendly and cost-effective way to prepare MNPs in nanoscale. This method mainly uses two different

approaches to reduce ferrous ion from $FeCl_3^-$ either Na_2SO_3 or $FeSO_4$. The later approach results in formation of rod shaped nanoparticles of over 30 nm. [24] Liposomal encapsulation of particles of this shape and size will have a greater impact on the overall size of MLs and may not be suitable for delivery across many physiological barriers such as BBB, stomach epithelial, etc. Most importantly, it may significantly downgrade the colloidal stability of MLs in the peripheral circulation. The Na_2SO_3-based reduction approach possesses advantage in producing round MNPs with smaller size, probably due to the gentle reduction ability from Na_2SO_3 in aqueous solution. Maghemite (Fe_2O_3) is the primary product of this reduction reaction which can be further oxidized under acidic condition resulting in Fe_3O_4 nanoparticles. As determined by TEM, ultrasmall magnetite nanoparticles of 7–10 nm possessing excellent dispersion property in aqueous medium which could be synthesized by this Na_2SO_3 reduction approach (Fig. 1a). These nano-sized particles possess remarkably higher specific surface area which improves drug loading ability and dissolution rate influencing the bioavailability. These particles could also manipulate and target at the sub-cellular organelles levels. The crystal structure of synthesized magnetite particles was confirmed by X-ray diffraction spectroscopic measurement (Fig. 1b). The X-ray spectrum consisted of magnetite-specific peaks which corresponded to 220, 311, 400, 511, and 440 planes. Magnetic hysteresis loops for these particles, which displayed strong magnetic property, were measured between +1200 to − 1200 Oersted (Oe).

As shown in Fig. 2a, the magnetization curves displayed no hysteresis, indicating a typical superparamagnetic behavior with no coercivity and remanence at room temperature. The superparamagnetism can be utilized for simultaneous monitoring and quantitation of MNPs distribution specific or nonspecific to various tissues. Meanwhile, quantitation of localization of MNPs associated drugs could be possible using techniques like magnetic resonance imaging (MRI) and magnetometery due to variation in the surface charge of naked and drug-bound nanoparticles, which leads a way for tracking the site-specific optimal or suboptimal drug-dosing. The surface charge of synthesized MNPs was determined by measuring the zeta-potential at different pH level in dispersion solution (Fig. 2b). Interestingly, with pH values changing from acidic to basic, zeta potential of MNPs alternated from positive charge of +26±1.5 mV at pH 4.75 to negative charge of −25±2.1 mV at pH 8.5. The isoelectric point of MNPs was determined at ~ pH 7.1. We noticed that content of dispersion solution also affects the surface charge of MNPs. As such, in Tris-EDTA buffer (pH 7.4), MNPs displayed zeta potential of approximately −23±1.2 mV which was nearly equivalent to that obtained in H_2O with pH 8.5 (−25±2.1 mV). Charges on the surface of Fe_3O_4 MNPs particles can be developed due to its amphoteric property in aqueous media. Acting as Lewis acid, at the hydrated solid/water interface, magnetite adsorb/coordinate water or hydroxyl group and gets H^+/OH^- ions along it surface. These ions can be replaced by other organic or organic anion, forming hydrogen bond, and adsorbs proton or cations. This could allow direct immobilization of various biomolecules/molecules on MNPs surface via hydrogen bonding, hydrophobic interaction, and electrostatic repulsion. [43–45] Also, the surface charge of magnetic nanoparticles may be converted either to positive or negative with different kinds of coating such as, the polyelectrolyte coating or silica layers, etc. [41; 46]

As stated earlier, one of the greatest challenges towards the successful application of MNPs in drug delivery is protection of associated drugs from enzymztic decomposition in blood circulation. Naked MNPs can interact with various plasma/serum proteins and may significantly affect the potential outcome of its applications in drug-related application such as target specificity, MRI, etc.[15; 24] It is true that liposomal encapsulation of MNPs is looked upon as potential solution of these concerns, while physiological integrity and stability of magneto-liposomal colloids needed to be addressed for their effective manipulation. Additionally, ways to maximize the target-reachability must be considered in the nano-formulated carrier. It has been suggested that modifications such as PEGlyation on liposomal surface may improve the inherent poor stability of conventional liposomes. Also, liposomal surface can be engineered for active targeting by applying surface modifications such as bioconjugation of antibodies/ligands specific to cells or tissues. Here, we used PEGylated lipid, DSPE-PEG, for liposome formulation. The PEG in this lipid was tethered to the hydrophilic head of phospholipid bilayer. Thus, upon liposomal formulation, PEG chain existed on the surface. In addition to provide colloidal stability, PEGylation may diminish protein-induced immunogenicity and could also reduce the uptake by reticuloendothelial system (RES) resulting in improving of plasma circulation time and increasing bioavailability of drug. [47; 48] To maximize the reachability of nanocarriers to the target i.e. in this case transportation across BBB, we embedded Transferrin, a ligand for the HBMVECs specific Transferrin receptor, on the surface of PEGylated ML. Presence of MNPs and BBB specific receptor's ligand on the same carrier could synergize the transmigration efficiency across BBB. Since the movement of MNPs will be influenced by external magnetic force, presence of ligand may add to this effect by providing uptake-specificity for BBB cells (in this case for HBMVECs). The ML possessing such dual targeting mechanisms could be epitomized for many other target-oriented deliveries. We further expanded this multifunctional ML by fluorescent labeling. This was achieved by adding green fluorescent tagged phosphatidylethanolamine, abbreviated as CFPE, in the liposomal formulation ingredients. Fluorescent moiety addition to ML could serve as a high sensitive tool for nanocarriers associated pharmacokinetics study such as quantification of cellular uptake or entrapment, tracking localization in tissues, etc. More importantly, incorporation of fluorescence in the MNPs-based nanocarriers provided two different imaging options, including MNPs-based MRI imaging and fluorescence-based optical imaging. We believe that easy availability of fluorescent-based imaging technique will widen the use of ML as convenience and cost-effective tools in the targeted-drug delivery with high efficiency.

Size of PEGylated ML nanocarriers formulated using extrusion technique was determined by DLS (Fig 3a) and further TEM was performed to visualize its composition (Fig 3b). As evident from both figures, the average diameter size of this nanoformulation was approximately 130±10 nm. Polydispersity index (PDI) of 0.10 suggested a very narrow size distribution range of this formulation. Encapsulation of MNPs into the liposomes was proved to be difficult task and a maximum of 15% EE had been shown earlier [36]. We here reported EE of 60.0% which could possibly be attributed to the ultrasmall sized MNPs. In the same line, TEM image (Fig 3b) showed that the ML formulation was filled with ultrasmall MNPs. For the figure 3b, it is true the lipids membrane was hard to be seen under

TEM. This is because of the low contrast difference between MNPs with bilayer of liposome. We tried to adjust the focus during performing TEM and stain the grid with phosphotungstic acid (2%), we still could not improve the quality. Although the visible liposome membrane could not be easily found in Figure 3b, the DLS data can verify the particles encapsulation inside liposome. It showed the size of MNPs without liposome encapsulation was only 10 nm and it turned out to be as 130 nm after liposomal encapsulation. These DLS sizes of MNPs with/without liposome encapsulation were showed in Figure 3a. In fact, as per the method adopted from our previous work, [49] which calculated the number of MNPs per liposomes, approximately 550 ultrasmall MNPs were estimated to be loaded in each liposome. Nonetheless, EE of ultrasmall MNPs in liposome could be manipulated by changing the ratio of particles with liposomes during the formulation process. Higher MNPs content may significantly improve the contrast enhancement effect of MRI in the future. Larger sized MNPs had been previously used due to their MR contrast enhancement effect. [22; 50] However, in view of transportability across BBB, smaller MNPs less than 10 nm may provide better pliant to liposomes, which could remarkably influence its transendothelial extravasation under external non-invasive magnetic force. More importantly, higher EE would provide higher number of MNPs per unit loading in one liposome resulting in significantly higher drug loading efficiency in single ML nanocarrier. According to the monogram-based theoretical calculation for liposomes surface area, [51] we estimated that one ml of unilamellar formulated liposomes suspension contained around 9×10^{13} magneto-liposomal carrier and their outer surface area was about 4.8 m^2. With such a higher concentration of ML, it is a challenge to maintain the mono-dispersibility of the nanocarriers. It becomes even more important in view of their potential application in targeted drug delivery. Although PEGylation adding to the colloidal stability can give assistance in maintaining the liposomal mono-dispersion, incubation temperature during the formulation process may also play a vital role. We achieved highly mono-dispersed liposomes using an incubation- and extrusion- temperature around ~40°C, which was higher than the thermogravimetric analysis points for all lipids ingredients. Homogenous size of ML nanocarriers was attained by using polycarbonate filter membrane of different pore-size (400 nm/200 nm/ 100 nm) during the extrusion procedure. Notably, molar concentration ratio of DSPE-PEG used during the formulation process was controlled less than 10% since a critical micelles concentration (CMC) limitation above which PEG influence the micelles formation. The formulated ML was subjected to DLS measurement and the zeta potential showed near neutral charge of −0.8±0.2 mV on the surface of these nanocarriers. Thus, possibility of charge-mediated cellular uptake of ML can be minimized in the peripheral circulation, while external magnetic force will remain the only controlling force of the nanocarriers for effective movement up to the target area.

In order to increase BBB specificity of the nanocarriers, Transferrin was embedded on their surface. Transferrin is one of rare proteins which have free access across the intact BBB and carry essential nutrients into the brain. Transferrin embedded on ML surface was confirmed by spectrophotometry (Fig 4). Similar to the previous study of Xu et al. [26], spectra of Transferrin embedded magnetic-liposomes showed red shift comparing with Transferrin. It should be noted that inclusion of less than 10% of PEG in formulation mixture results in homogenous PEGylation rather than forming thick corona which was noticed in the work of

Gao et al. [23] The shielding effect thick PEG corona may cause improper ligand bind and also may prevent proper interaction of ligand to the receptor on the cells. In other hand, the homogenous grafting of 2000 Da PEG on the ML surface may have negligible interference during the recognition of 80 kDa Transferrin from its cellular receptors. Similarly, homogenous Transferrin distribution should not affect the original objective of PEG in providing colloidal stability. As determined by DLS, Transferrin embedding to the ML surface has no significant effect on its hydrodynamic size or surface charge. The nanocarrier diameter increased slightly up to 136±11 nm from 130±10 nm. The PDI was 0.18 which again suggested a narrow size distribution range of this formulation.

The formulated ML nanocarriers were assessed for its sustainability in the physiological equivalent temperature and circulation. Nanocarriers suspended in the PBS were incubated in 37°C for up to 30 hours and their sizes were measured by DLS at different time points. As shown in Figure 5a, size of these formulations remained almost unchanged. Similarly, fluorescent intensity emitted from equal amount of ML carriers kept constant through-out the incubation period (Fig. 5a). It should be noted that fluorescent integration in ML enriched its multifunction such as easily manageable quantification and visualization of carriers during experimental settings. This was achieved by adding green fluorescent tagged lipid, namely CFPE, in the liposomal formulation mixture. Sustainability of these carriers was further evaluated in the *in vitro* closed circulation system which consists of a bidirectional, self-priming peristaltic capillary pump. A schematic of this pump was shown in Figure 5b. Here also, both, the structural integrity and fluorescent intensity of ML nanocarriers remained unaffected through 120 equivalent blood-circulations of experimental settings (Fig. 5c). Fluorescent intensity study together with the DLS measurement showed that the formulated ML nanocarriers could sustain its structural integrity in the simulated blood circulation and physiological temperature for considerable amount of time. This suggested toward the possible use of fluorescent ML nanocarriers for *in vivo* drug delivery and optical imaging. Nanocarriers were also displayed their storage durability at 4°C for around one month. Again, constant diameters were determined throughout the storage period (Fig. 5d). Also, as expected, hydrodynamic difference between the diameter of Transferrin embedded or non-embedded liposomes remained less than 10 % throughout the storage time. Nonetheless, it was worth mentioning that the colloidal stability and optical properties of the ML nanocarriers remained unaffected due Transferrin embedding. These phenomena suggested that the ML nanocarriers possessed longer storage stability and drugs loaded on these carriers could have minimum leaching effect. In fact, consistent fluorescent intensity either during exposure of physiological temperature, peristaltic circulation or storage implied toward minimum leakage from formulated ML nanocarriers. Figure 5e and 5f respectively showed the appearance of suspended ML nanoformulations after one month of storage at 4°C in the absence and presence of magnetic force. Larger size MNPs (35 nm) were also tested for encapsulation in the liposomes. However, the problem of stability and precipitation remained an big issue because ML could not sustain in suspension for even couple of hours.

Finally, the BBB transmigrability of the ML nanocarriers was evaluated using an *in vitro* BBB model composed by human brain sourced primary cells. As described previously, [39]

BBB model was established with a bi-compartmentalized transwell where HBMECs and HAs were grown to confluence on the upper chamber and underside of lower chamber respectively. The intactness of grown BBB could be evaluated by TEER measurement. A TEER value of ~200 ohms/cm^2 comparing to the control (non-cultured wells) was considered consistent with the formation of intact BBB. Following the TEER determination, Transferrin embedded or non-embedded fluorescent ML nanocarriers were subjected to different wells either in presence or absence of external magnetic force. As shown in Table 1initial TTER values of all treatment groups were close to standard 200 ohms/cm^2. A schematic of proposed mechanism of transmigration across BBB was depicted in Figure 6.

As expected, comparing to the individual effect of magnetic force- and Transferrin receptor-mediated transportation, significantly higher transmigration of MLs nanocarriers were detected across BBB due to their synergic effect (Fig. 7a & b). Incorporation of fluorescence in the ML nanocarrier was used for quantifying its transmigration from apical to basolateral layers in the BBB model. From Figure 7a, Transferrin embedded ML nanocarriers in presence of external magnetic force (Tf.ML + force) showed higher transmigration than other treatment groups from as early as 4–6 hours of experimental period. Approximately 50% increased transmigration was achieved due to synergy effect (Tf.ML + force) in compare to ML nanocarriers deprived of only Transferrin and magnetic force and this continued till 24 hours of experimental period (Fig. 7b). Similarly, Transferrin embedded ML nanocarriers in absence of magnetic force (Tf.ML) showed approximately 25–35% less transmigration than synergy effect (Tf.ML + force) throughout the experimental period (Fig. 7b). Interestingly, presence of external magnetic force did not affect the transmigration for at least first 6 hour in Transferrin embedded (Tf.ML + force) or non-embedded (ML + force) ML nanocarrier (Fig. 7a & 7b). However, 25%-30% increased transmigration was noticed between 12–24 hours of experimental period (Fig. 7b). This increased transmigration from 6 hours post-treatment due to synergy effect (Tf.ML + force) could be explained by the fact that the rate of receptor mediated transportation by BBB cells may accelerate along with time. While it may occur at slower rate in the beginning, increased cellular uptake and accumulation of ML nanocarriers during late phase may speed up transportation mediation via receptor. As such, sudden increase in transmigration was seen after 4–6 hr of treatment. Consistent exposure of a defined magnetic force should result in constant transmigration. In fact, comparing the “ML+Force” and “Tf.ML” group, reversal of transmigration trend was found at time of 16 hours post-treatment (Fig. 7a). While constant but higher transmigration trend was evident for “ML+Force” group (i.e. effect of external magnetic force) than “Tf.ML” group till 12 hour, higher transmigration for “Tf.ML” group post 16 hour suggested influence of receptor mediated transportation during late phase. Overally, independent of Transferrin embedding, groups with external magnetic force showed higher transmigration in compare with the groups without this force after approximately 4 hours post-treatments onwards for major part of experimental period. It could possible that magnetic force may allow transient change in BBB permeability resulting in increasing transendothelial extravasation of ML nanocarriers. Magnetic force induced alteration of BBB permeability in a reversal way had been reported before. Working with the Fe_3O_4-PEG nanocarriers, Gao et al showed an alteration in BBB permeability after 4 hours of exposure. [22] Similarly, treatment of polysorbate derived nanoparticles resulted in sharp increase in

permeability from 4–7 hours and accordingly TEER values were reversed from less to high.[52]

In our study, TEER values of BBB remained close to the standard 200 ohms/cm^2 both at the beginning and end of experimental period, suggesting unaffected integrity of BBB due to exposure of different nanoformulations (Table 1). The transmigration pattern of different experimental groups was further verified by measuring the cellular iron concentration. Triton mediated liposomes or cells breaking results in release of encapsulated and/or uptake Fe_3O_4 which was exposed to ammonium thiocyanate following oxidation via ammonium persulfate. Quantification of resulting iron-thiocyanate emitting red color at 490 nm provided concentration of Fe_3O_4 uptake by BBB cells. The evidence from Figure 8consistent with the maximum transmigrability, synergic effect (Tf.ML + force) showed highest iron concentration. These results supported our observation that synergy may result in increased accumulation of ML nanocarriers at the BBB causing higher transendothelial extravasation and/or receptor-mediated transmigration. As expected, lowest iron concentration was found in BBB cells exposed to ML nanocarriers deprived of both Transferrin and magnetic force. Since iron oxide nanoparticles were encapsulated inside liposome and this liposomal structure will not break down during the transmigration BBB membrane,[22] so the ratio of Fe (or Fe ions) in basal chamber to that of apical chamber can be controlled by the external magnetic force and the performance time. The pattern of Fe_3O_4 uptake was further verified by confocal microscopy. Again, we saw that synergic effect (Tf.ML + force) resulted in highest and more uniform luminescence pattern in endothelial cells (Fig. 9a) in compare to “ML+Force” (Fig. 9b)"Tf.ML” (Fig. 9c), and “ML” (Fig. 9d) groups. This consistent fluorescent pattern together with the iron concentration supported our notion that while external magnetic force alone may influence the BBB transmigrability of ML nanocarriers, addition of ligand to the nanocarriers may synergize this effect via receptor mediation transportation. More importantly, cytotoxicity studies of astrocytes and HBMVE cells showed the non-toxicity effect on cells from our nanocarriers (Fig. 10). In the same line it suggested that doses of MNPs within the permissible limitation had non-significant safety concerns and were biocompatible.

Overall, this ML nanoformulation displayed significant synergic effect on BBB transmigration with dual mechanism of receptor-mediation and external non-invasive magnetic force. It embraced the great potential to be used as carrier for drug delivery across BBB. In our design, liposome was used not only to encapsulate the magnetic nanoparticles, but also protect the bounded drugs from degradation before reaching the target site or lesions. The bilayer structure of liposome will remain intact during crossing the BBB membrane, and will not affect the final integrity of BBB membrane, which was confirmed by transendothelial electrical resistance (TEER) values.[22] Since the relatively weak external magnetic force (0.08 Tesla) was used in our study, once the strong permanent magnet (1.0 Tesla or higher) is employed, this multiple functional ferrous liposomal nanoformulation can be applied not only *in vitro* and also *in vivo*. Because of the specific surface charge on MNPs, anti-retroviral (ARV) drugs may be designed to be bound on the surface for target drug delivery. And also, the ferrous surface of MNPs may be coated with high conductivity and high biocompatible rare metal layer (for example, gold, silver etc.) for

the future controlled drug release. Since our research group has already been equipped with MRI instrument, the incorporation of MRI imaging derived from ferrous composition is our next theranostic study plan, which can forward our BBB transmigration study from *in vitro* to *in vivo* status in our lab and university animal facility.

4. Conclusion

Almost all CNS-related disease remains untreated, mainly due to limited permeability of endogenous or exogenous molecules across BBB. In the wake of fact that 98 % drugs do not reach in the brain, MNPs-based approach may provide a viable options for safe, effective and target-specific drug-delivery. Importantly, MNPs could serve as an integrated platform for targeting, imaging, and therapy, which is the basis of recently conceptualized theranostic nanomedicine. As such, exploring the potential of MNPs for brain drug delivery, we, herein, for the first time reported ultrasmall MNPs-based nanocarrier, namely ML, possessing two means of transportation across BBB. Our results showed that incorporation of receptor mediated targeting with external magnetic force had successfully led to higher transendothelial migration of ML nanocarrier than their individual effect. While either of receptor-mediation or external non-invasive magnetic force may certainly improve the BBB delivery of ML nanocarriers in compare with the traditional methods, their conjugation on the same ML nanocarriers became more important in context to their escape from reticuloendothelial uptake. As happened with other cases, sole dependence on receptor-mediated brain targeting may not be feasible due to probable engulfment of nanocarriers by reticuloendothelial system. This uncertainty- if and when nanocarrier reached the brain- could be minimized by addition of MNPs because its movement can be remotely controlled by external magnetic force. Thus, MNPs based nanocarriers could reach brain within short time, where, in addition to transendothelial extravasation, presence of ligand on carrier may influence receptor-mediated transmigration. Nonetheless, *in vivo* research-homework need to be elucidated and molecular mechanism behind this dual transportation mechanism is required to be addressed for successful application of the nanocarriers in treatment of different CNS diseases.

Acknowledgement

This work was supported by NIH grant 1R01DA027049 (PI: Dr. Madhavan P. Nair). We also would like to appreciate the assistance of Dr. Yong Cai, Department of Chemistry and Biochemistry, Florida International University, for the DLS measurement, and that of Dr. Andriy Durygin, CeSMEC center, Florida International University, for the XRD assay.

Abbreviations

BBB	Blood-brain barrier
BMECs	brain microvascular endothelial cells
Chol	cholesterol
CMC	critical micelles concentration

CFPE	1,2-distearoyl-sn-glycero-3-phosphoethnolamine-N-carboxylfluorescein
CNS	central nervous system
DLS	dynamic laser scattering
EE	encapsulation efficiency
EPC	egg phosphatidylcholine
HA	human brain astrocytes
HMBVEC	human brain endothelial cell
Fe3O4	Iron oxide
Lf	lactoferrin
MNPs	magnetic nanoparticles
ML	magneto liposome
ML+Force	only magnetic force on magneto-liposome
MRI	magnetic resonance imaging
MTS	[3-(4, 5-dimethyl thiazol-2-yl)-5-(3-carboxy-methoxyphenyl)-2-(4-sulfophenyl)-2H-tetrazolium, inner salt
PEG	poly(ethylene glycol)
mPEG2000-DSPE	1,2-distearoyl-sn-glycero-3-phosphoethnolamine-N-[methyoxy(polyethylene glycol)-2000]
RES	reticuloendothelial system
SD	standard derivation
SPOI	superpara-magnetic iron oxide
TEER	transendothelial electrical resistance
TEM	transmission electron microscopy
Tf	Transferrin
Tf.ML + force	both transferrin and external magnetic force on magneto-liposome
Tf.ML	only transferrin embedded magneto-liposome
USPIO	ultrasmall superparamagnetic iron oxide
XRD	X-ray diffraction

References

1. Bogich TL, Chunara R, Scales D, Chan E, Pinheiro LC, Chmura AA, Carroll D, Daszak P, Brownstein JS. Preventing pandemics via international development: A systems approach. PLoS Med. 2012; 9(12):e1001354. [PubMed: 23239944]

2. Pardridge WM. The Blood-Brain Barrier: Bottleneck in Brain Drug Development. NeuroRx. 2005; 2(1):3–14. [PubMed: 15717053]
3. Pardridge WM. Drug transport across the blood-brain barrier. J Cereb Blood Flow Metab. 2012; 32(11):1959–1972. [PubMed: 22929442]
4. Le Douce V, Herbein G, Rohr O, Schwartz C. Molecular mechanisms of HIV-1 persistence in the monocyte-macrophage lineage. Retrovirology. 2010; 7(1):32. [PubMed: 20380694]
5. Batrakova EV, Gendelman HE, Kabanov AV. Cell-mediated drug delivery. Expert Opinion on Drug Delivery. 2011; 8(4):415–433. [PubMed: 21348773]
6. Ding H, Wu F. Image guided biodistribution and pharmacokinetic studies of theranostics. Theranostics. 2012; 2(11):1040–1053. [PubMed: 23227121]
7. Atluri VSR, Kanthikeel SP, Reddy PVB, Yndart A, Nair MPN. Human Synaptic Plasticity Gene Expression Profile and Dendritic Spine Density Changes in HIV-Infected Human CNS Cells: Role in HIV-Associated Neurocognitive Disorders (HAND). PLoS One. 2013; 8(4):e61399. [PubMed: 23620748]
8. Pardridge WM. Biopharmaceutical drug targeting to the brain. Journal of Drug Targeting. 2010; 18(3):157–167. [PubMed: 20064077]
9. Verma S, Lo Y, Chapagain M, Lum S, Kumar M, Gurjav U, Luo H, Nakatsuka A, Nerurkar VR. West Nile virus infection modulates human brain microvascular endothelial cells tight junction proteins and cell adhesion molecules: Transmigration across the in vitro blood-brain barrier. Virology. 2009; 385(2):425–433. [PubMed: 19135695]
10. Ding H, Wu F. Image guided biodistribution of drugs and drug delivery. Theranostics. 2012; 2(11): 1037–1039. [PubMed: 23227120]
11. Nair SB, Dileep A, Rajanikant GK. Nanotechnology based diagnostic and therapeutic strategies for neuroscience with special emphasis on ischemic stroke. Current Medicinal Chemistry. 2012; 19(5):744–756. [PubMed: 22204347]
12. Bonoiu AC, Mahajan SD, Ding H, Roy I, Yong K-T, Kumar R, Hu R, Bergey EJ, Schwartz SA, Prasad PN. Nanotechnology approach for drug addiction therapy: Gene silencing using delivery of gold nanorod-siRNA nanoplex in dopaminergic neurons. Proceedings of the National Academy of Sciences. 2009; 106(14):5546–5550.
13. Ding H, Wu F, Nair MP. Image-guided drug delivery to the brain using nanotechnology. Drug Discovery Today. 2013; 18(21–22):1074–1080. [PubMed: 23817076]
14. Liu L, Ding H, Yong K-T, Roy I, Law W-C, Kopwitthaya A, Kumar R, Erogbogbo F, Zhang X, Prasad P. Application of Gold Nanorods for Plasmonic and Magnetic Imaging of Cancer Cells. Plasmonics. 2011; 6(1):105–112.
15. Sun C, Lee JSH, Zhang M. Magnetic nanoparticles in MR imaging and drug delivery. Advanced Drug Delivery Reviews. 2008; 60(11):1252–1265. [PubMed: 18558452]
16. Veiseh O, Gunn JW, Zhang M. Design and fabrication of magnetic nanoparticles for targeted drug delivery and imaging. Advanced Drug Delivery Reviews. 2010; 62(3):284–304. [PubMed: 19909778]
17. Zhen Z, Xie J. Development of manganese-based nanoparticles as contrast probes for magnetic resonance imaging. Theranostics. 2012; 2(1):45–54. [PubMed: 22272218]
18. Boado RJ, Hui EKW, Lu JZ, Sumbria RK, Pardridge WM. Blood-Brain Barrier Molecular Trojan Horse Enables Imaging of Brain Uptake of Radioiodinated Recombinant Protein in the Rhesus Monkey. Bioconjugate Chemistry. 2013; 24(10):1741–1749. [PubMed: 24059813]
19. Roy U, Bulot C, Honer zu Bentrup K, Mondal D. Specific Increase in MDR1 Mediated Drug-Efflux in Human Brain Endothelial Cells following Co-Exposure to HIV-1 and Saquinavir. PLoS One. 2013; 8(10):e75374. [PubMed: 24098380]
20. Ding H, Yong K-T, Roy I, Hu R, Wu F, Zhao L, Law W-C, Zhao W, Ji W, Liu L, Bergey EJ, Prasad PN. Bioconjugated PLGA-4-arm-PEG branched polymeric nanoparticles as novel tumor targeting carriers. Nanotechnology. 2011; 22(16):165101. [PubMed: 21393821]
21. Pilakka-Kanthikeel S, Atluri VSR, Sagar V, Saxena SK, Nair M. Targeted Brain Derived Neurotropic Factors (BDNF) Delivery across the Blood-Brain Barrier for Neuro-Protection Using Magnetic Nano Carriers: An In-Vitro Study. PLoS One. 2013; 8(4):e62241. [PubMed: 23653680]

22. Qiao R, Jia Q, Hüwel S, Xia R, Liu T, Gao F, Galla H-J, Gao M. Receptor- Mediated Delivery of Magnetic Nanoparticles across the Blood–Brain Barrier. ACS Nano. 2012; 6(4):3304–3310. [PubMed: 22443607]
23. Kaasgaard T, Mouritsen OG, Jørgensen K. Screening effect of PEG on avidin binding to liposome surface receptors. International Journal of Pharmaceutics. 2001; 214(1–2):63–65. [PubMed: 11282238]
24. Saiyed ZM, Gandhi NH, Nair MP. Magnetic nanoformulation of azidothymidine 5'-triphosphate for targeted delivery across the blood–brain barrier. International Journal of Nanomedicine. 2010; 5:157–166. [PubMed: 20463931]
25. Safinya CR, Ewert KK. Materials chemistry: Liposomes derived from molecular vases. Nature. 2012; 489(7416):372–374. [PubMed: 22996547]
26. Peng A, Kosloski M, Nakamura G, Ding H, Balu-Iyer S. PEGylation of a Factor VIII–Phosphatidylinositol Complex: Pharmacokinetics and Immunogenicity in Hemophilia A Mice. The AAPS Journal. 2012; 14(1):35–42. [PubMed: 22173945]
27. Nie Y, Ji L, Ding H, Xie L, Li L, He B, Wu Y, Gu Z. Cholesterol derivatives based charged liposomes for doxorubicin delivery: preparation, in vitro and in vivo characterization. Theranostics. 2012; 2(11):1092–1103. [PubMed: 23227125]
28. Xie J, Lee S, Chen X. Nanoparticle-based theranostic agents. Advanced Drug Delivery Reviews. 2010; 62(11):1064–1079. [PubMed: 20691229]
29. Torchilin VP, Levchenko TS, Rammohan R, Volodina N, Papahadjopoulos-Sternberg B, D'Souza GGM. Cell transfection in vitro and in vivo with nontoxic TAT peptide-liposome– DNA complexes. Proceedings of the National Academy of Sciences. 2003; 100(4):1972–1977.
30. Sloat B, Cui Z. Strong mucosal and systemic immunities induced by nasal immunization with anthrax protective antigen protein incorporated in liposome-protamine-DNA particles. Pharmaceutical Research. 2006; 23(2):262–269. [PubMed: 16319999]
31. Dykxhoorn DM, Palliser D, Lieberman J. The silent treatment: siRNAs as small molecule drugs. Gene Ther. 2006; 13(6):541–552. [PubMed: 16397510]
32. Ulbrich K, Hekmatara T, Herbert E, Kreuter J. Transferrin- and transferring-receptor- antibody-modified nanoparticles enable drug delivery across the blood–brain barrier (BBB). European Journal of Pharmaceutics and Biopharmaceutics. 2009; 71(2):251–256. [PubMed: 18805484]
33. Moos T, Morgan E. Transferrin and Transferrin receptor function in brain barrier systems. Cellular and Molecular Neurobiology. 2000; 20(1):77–95. [PubMed: 10690503]
34. Hu K, Li J, Shen Y, Lu W, Gao X, Zhang Q, Jiang X. Lactoferrin-conjugated PEG–PLA nanoparticles with improved brain delivery: In vitro and in vivo evaluations. Journal of Controlled Release. 2009; 134(1):55–61. [PubMed: 19038299]
35. Sun, Y-k; Ma, M.; Zhang, Y.; Gu, N. Synthesis of nanometer-size maghemite particles from magnetite. Colloids and Surfaces A: Physicochemical and Engineering Aspects. 2004; 245(1–3): 15–19.
36. Deng L, Ke X, He Z, Yang D, Gong H, Zhang Y, Jing X, Yao J, Chen J. A MSLN-targeted multifunctional nanoimmunoliposome for MRI and targeting therapy in pancreatic cancer. International Journal of Nanomedicine. 2012; 7:5053–5065. [PubMed: 23028227]
37. Xu G, Yong K-T, Roy I, Mahajan SD, Ding H, Schwartz SA, Prasad PN. Bioconjugated quantum rods as targeted probes for efficient transmigration across an in vitro blood–brain barrier. Bioconjugate Chemistry. 2008; 19(6):1179–1185. [PubMed: 18473444]
38. Gandhi N, Saiyed ZM, Napuri J, Samikkannu T, Reddy PV, Agudelo M, Khatavkar P, Saxena SK, Nair MP. Interactive role of human immunodeficiency virus type 1 (HIV-1) clade-specific Tat protein and cocaine in blood-brain barrier dysfunction: Implications for HIV-1–associated neurocognitive disorder. Journal of Neurovirology. 2010; 16(4):294–305. [PubMed: 20624003]
39. Frascione D, Diwoky C, Almer G, Opriessnig P, Vonach C, Gradauer K, Leitinger G, Mangge H, Stollberger R, R P. Ultrasmall superparamagnetic iron oxide (USPIO)-based liposomes as magnetic resonance imaging probes. International Journal of Nanomedicine. 2012; 7(1):2349–2359. [PubMed: 22661890]
40. Zhu X-M, Wang Y-XJ, Leung KC-F, Lee S-F, Zhao F, Wang D-W, Lai JM, Wan C, Cheng CH, Ahuja AT. Enhanced cellular uptake of aminosilane-coated superparamagnetic iron oxide

nanoparticles in mammalian cell lines. International Journal of Nanomedicine. 2012; 7:953–964. [PubMed: 22393292]

41. Ding H, Yong K-T, Roy I, Pudavar HE, Law WC, Bergey EJ, Prasad PN. Gold nanorods coated with multilayer polyelectrolyte as contrast agents for multimodal imaging. The Journal of Physical Chemistry C. 2007; 111(34):12552–12557.
42. Jayapaul J, Hodenius M, Arns S, Lederle W, Lammers T, Comba P, Kiessling F, Gaetjens J. FMN-coated fluorescent iron oxide nanoparticles for RCP-mediated targeting and labeling of metabolically active cancer and endothelial cells. Biomaterials. 2011; 32(25):5863–5871. [PubMed: 21605902]
43. Peng ZG, Hidajat K, Uddin MS. Adsorption of bovine serum albumin on nanosized magnetic particles. Journal of Colloid and Interface Science. 2004; 271(2):277–283. [PubMed: 14972603]
44. Homola A, James RO. Preparation and characterization of amphoteric polystyrene latices. Journal of Colloid and Interface Science. 1977; 59(1):123–134.
45. Yu S, Wu G, Gu X, Wang J, Wang Y, Gao H, Ma J. Magnetic and pH-sensitive nanoparticles for antitumor drug delivery. Colloids and Surfaces B: Biointerfaces. 2013; 103(0):15–22. [PubMed: 23201714]
46. Gittins DI, Caruso F. Tailoring the polyelectrolyte coating of metal nanoparticles. The Journal of Physical Chemistry B. 2001; 105(29):6846–6852.
47. Nie Y, Zhang Z, Li L. Synthesis, characterization and transfection of a novel folatetargeted multipolymeric nanoparticles for gene delivery. Journal of Materials Science: Materials in Medicine. 2009; 20(9):1849–1857. [PubMed: 19418206]
48. Ding H, Wu F, Huang Y, Zhang Z-r, Nie Y. Synthesis and characterization of temperature-responsive copolymer of PELGA modified poly(N-isopropylacrylamide). Polymer. 2006; 47(5): 1575–1583.
49. Ding H, Yong K-T, Law W-C, Roy I, Hu R, Wu F, Zhao W, Huang K, Erogbogbo F, Bergey EJ, Prasad PN. Non-invasive tumor detection in small animals using novel functional Pluronic nanomicelles conjugated with anti-mesothelin antibody. Nanoscale. 2011; 3(4):1813–1822. [PubMed: 21365120]
50. Jun, Y-w; Huh, Y-M.; Choi, J-s; Lee, J-H.; Song, H-T.; KimKim, Yoon, S.; Kim, K-S.; Shin, J-S.; Suh, J-S.; Cheon, J. Nanoscale Size Effect of Magnetic Nanocrystals and Their Utilization for Cancer Diagnosis via Magnetic Resonance Imaging. Journal of the American Chemical Society. 2005; 127(16):5732–5733. [PubMed: 15839639]
51. Torchilin, V.; Weissig, V. Liposomes: A Practical Approach. Oxford University Press; 1990.
52. Rempe R, Cramer S, Hüwel S, Galla H-J. Transport of Poly(n-butylcyano-acrylate) nanoparticles across the blood–brain barrier in vitro and their influence on barrier integrity. Biochemical and Biophysical Research Communications. 2011; 406(1):64–69. [PubMed: 21295549]

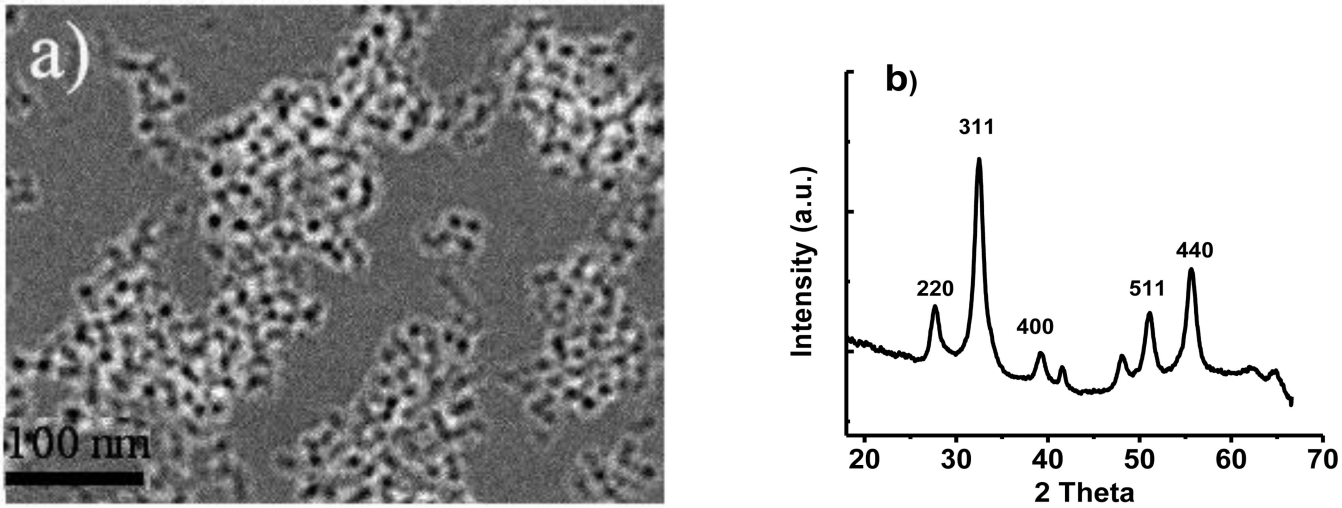

Figure 1.

Characterization of ultrasmall magnetite nanoparticles: a) TEM image showed MNPs of 7–10 nm. b) XRD spectrum showed magnetite-specific characteristics plane.

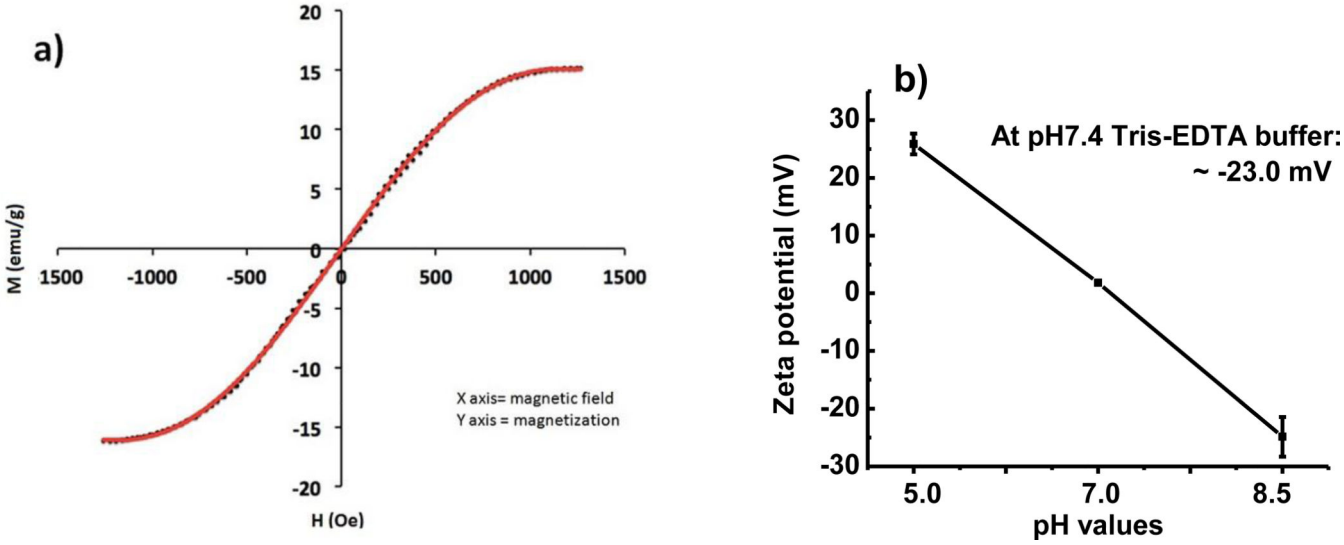

Figure 2.

a) Magnetic hysteresis loop of MNPs showed no coercivity and remanence at room temperature suggested its superparamagnetic behavior. b) Surface charge of MNPs varied according to pH values of suspension solution. At pH7.4 of Tris-EDTA buffer, it showed the zeta potential as −23.0 mV

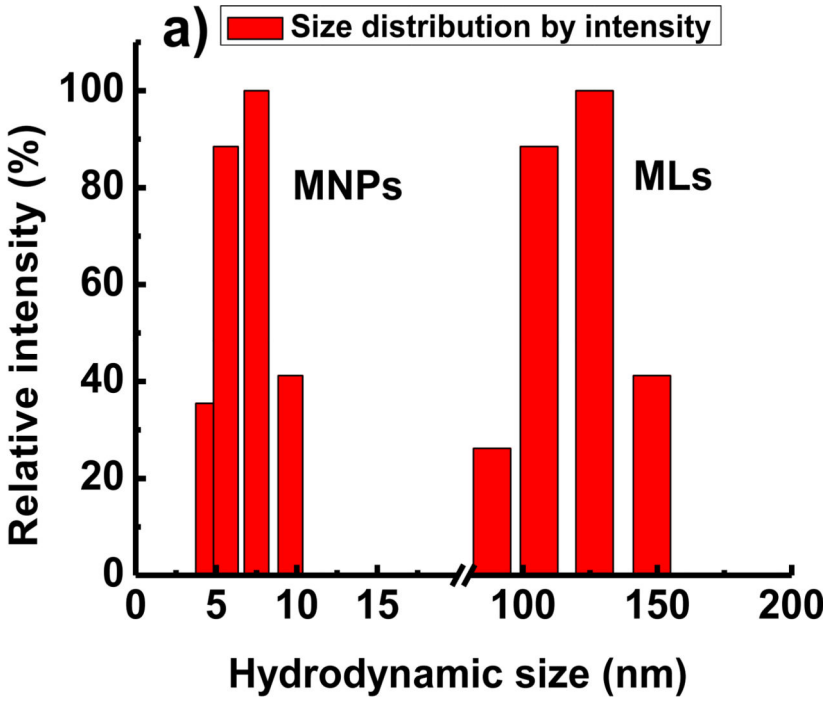

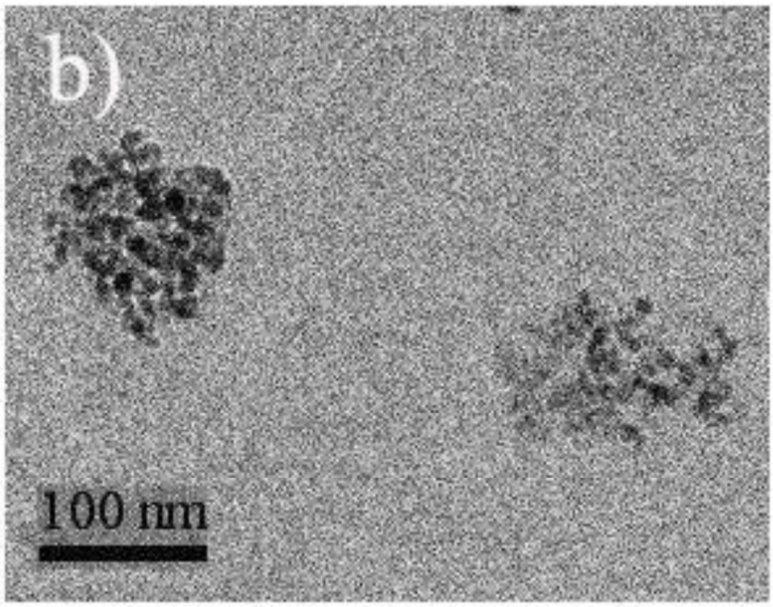

Figure 3.

Characterization of magnetic-liposomes (MLs): a) Dynamic laser scattering (DLS) measurement of hydrodynamic size distribution of MNPs and MLs. Average diameter size of this nanoformulation was approximately 7.5±1.8nm and 130±10 nm for MNPs and MLs, respectively. b) TEM image of ML nanocarriers containing MNPs (black dots) determined by DLS measurement.

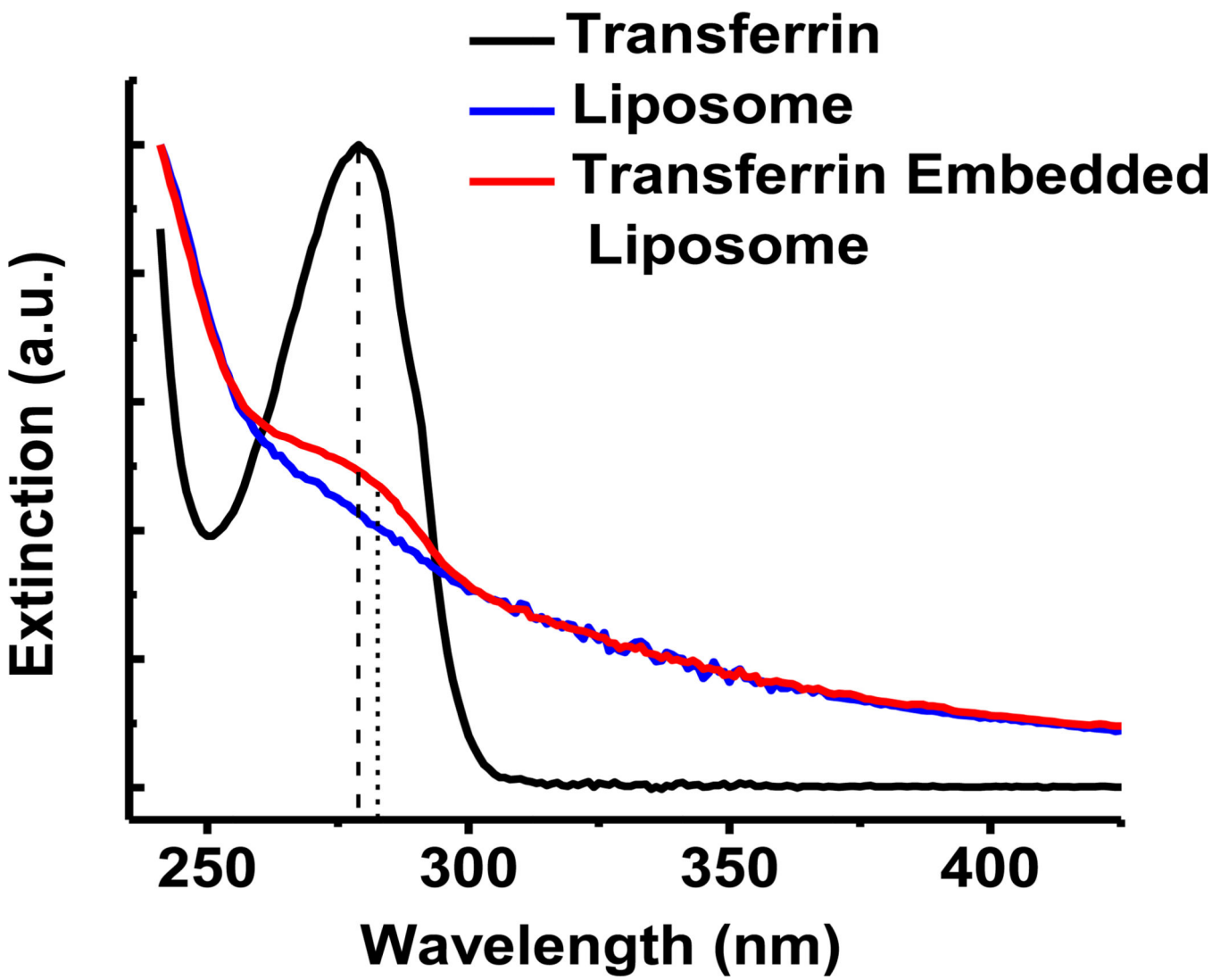

Figure 4.
Characterization of transferrin embedded in ML: spectra of transferrin embedded MLs showed red shift of peak comparing with Transferrin.

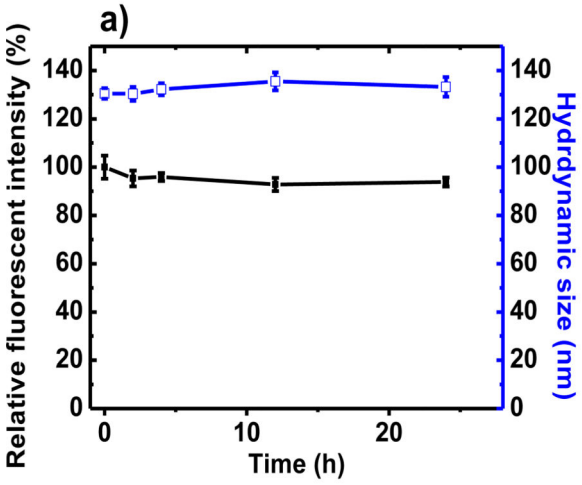

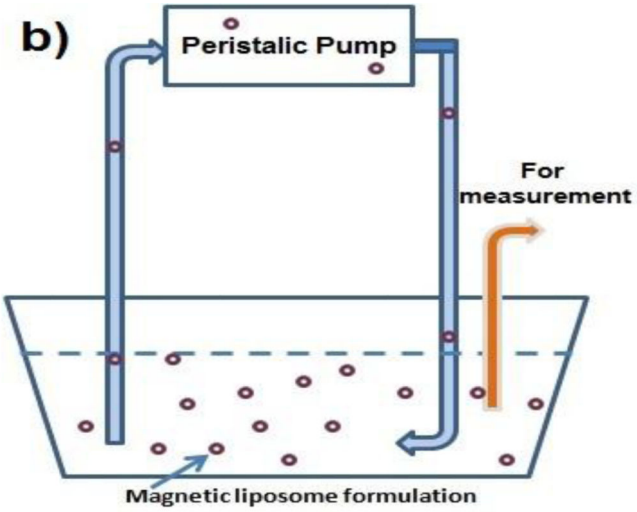

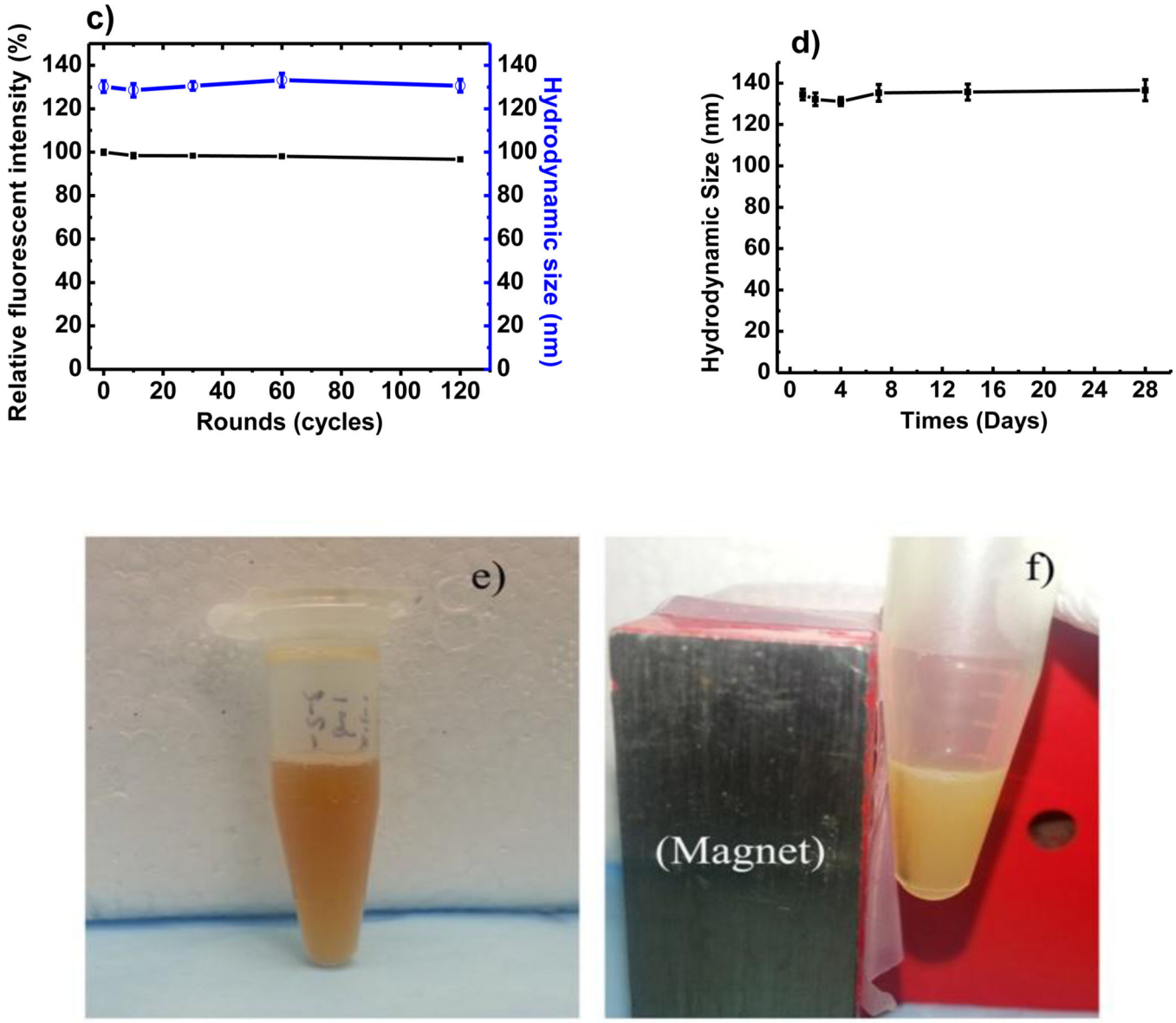

Figure 5.

Characterization of MLs sustainability: a) Fluorescent intensity (black) and average diameter (Blue) of ML nanoformulations incubated at 37°C. It suggested that structural integrity and fluorescent intensity of ML nanocarriers remained unaffected up to 30 hrs of experimental period. b) Schematic of *in vitro* closed circulation system: the bidirectional, self-priming peristaltic capillary pump simulated physiological equivalent blood-circulation. c) Fluorescent intensity (black) and average diameter (Blue) of ML nanoformulations after various round of *in-vitro* circulations. It suggested that structural integrity and fluorescent intensity of ML nanocarriers remained unaffected up to 120 circulations of experimental period. d) Average diameter (Blue) of ML nanoformulations in storage at 4°C suggested its structural integrity up to 28 days of experimental duration. e) Suspension of ML nanoformulations after one month of storage at 4°C. e) Suspension of ML nanoformulations after one month of storage at 4°C in the presence of magnetic force.

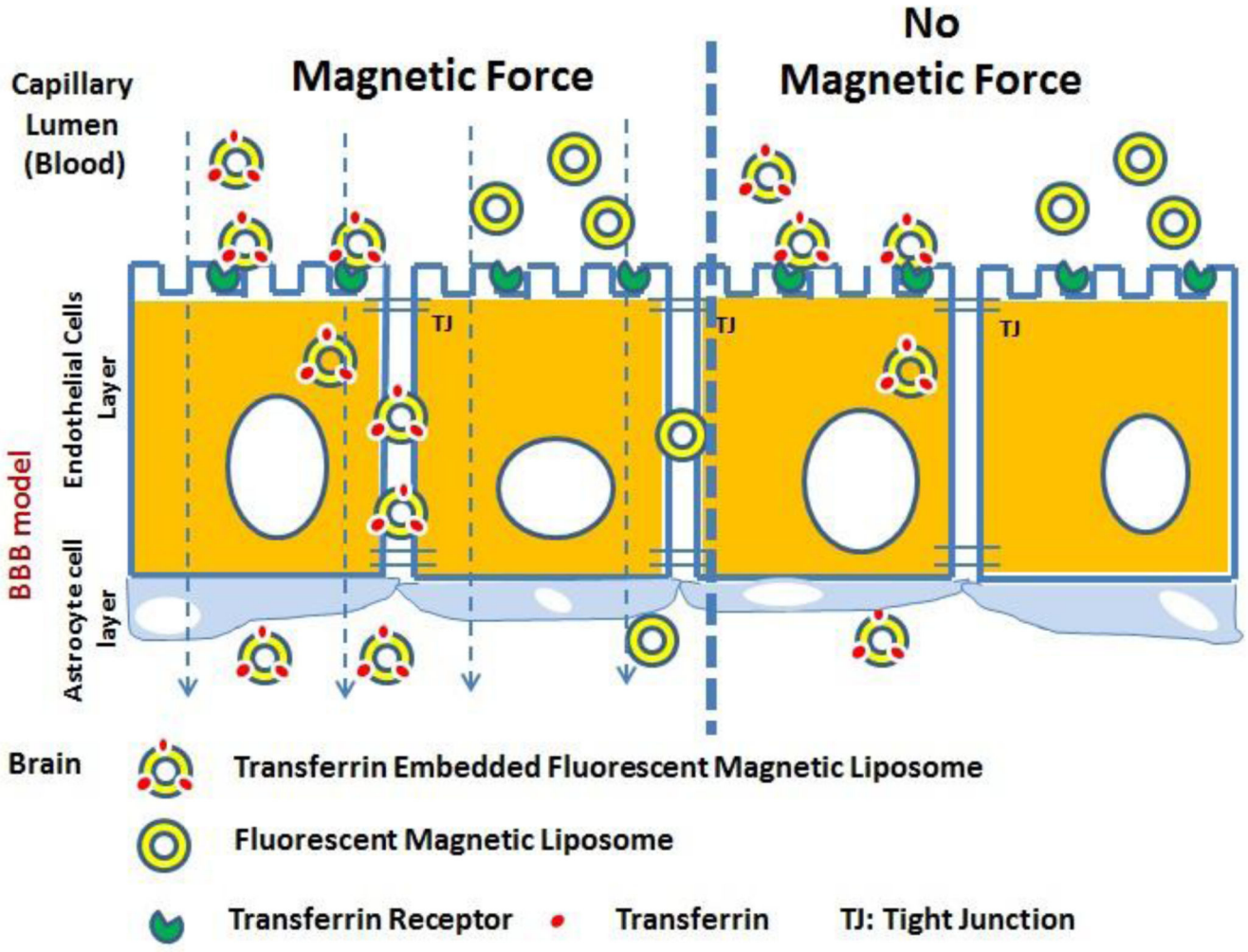

Figure 6.

Schematic of proposed mechanism of BBB transmigration of Transferrin embedded and non-embedded ML nanocarriers in the presence and absence of external magnetic force In compare to the individual effect of magnetic force- and Transferrin receptor- mediated transportation, significantly higher transmigration of ML nanocarriers across BBB was expected due to their synergy.

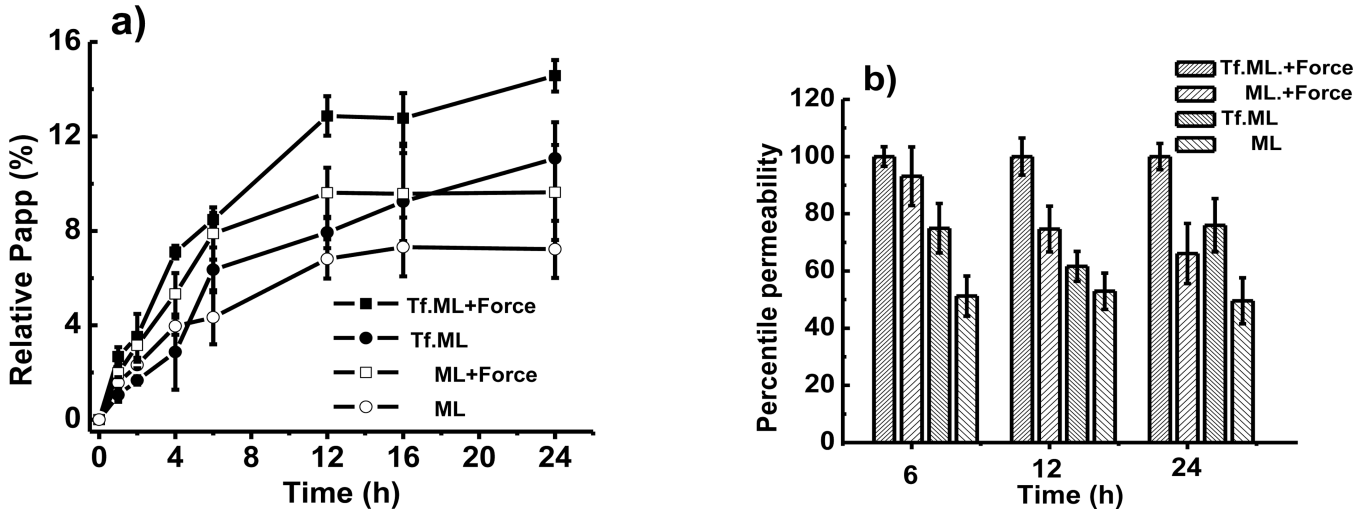

Figure 7.

a) Relative apparent permeability (Papp) of Transferrin embedded and non-embedded ML nanocarriers in the presence and absence of external magnetic force across *in vitro* BBB. b) Percentile permeability of different groups at 6, 12 and 24 hrs.

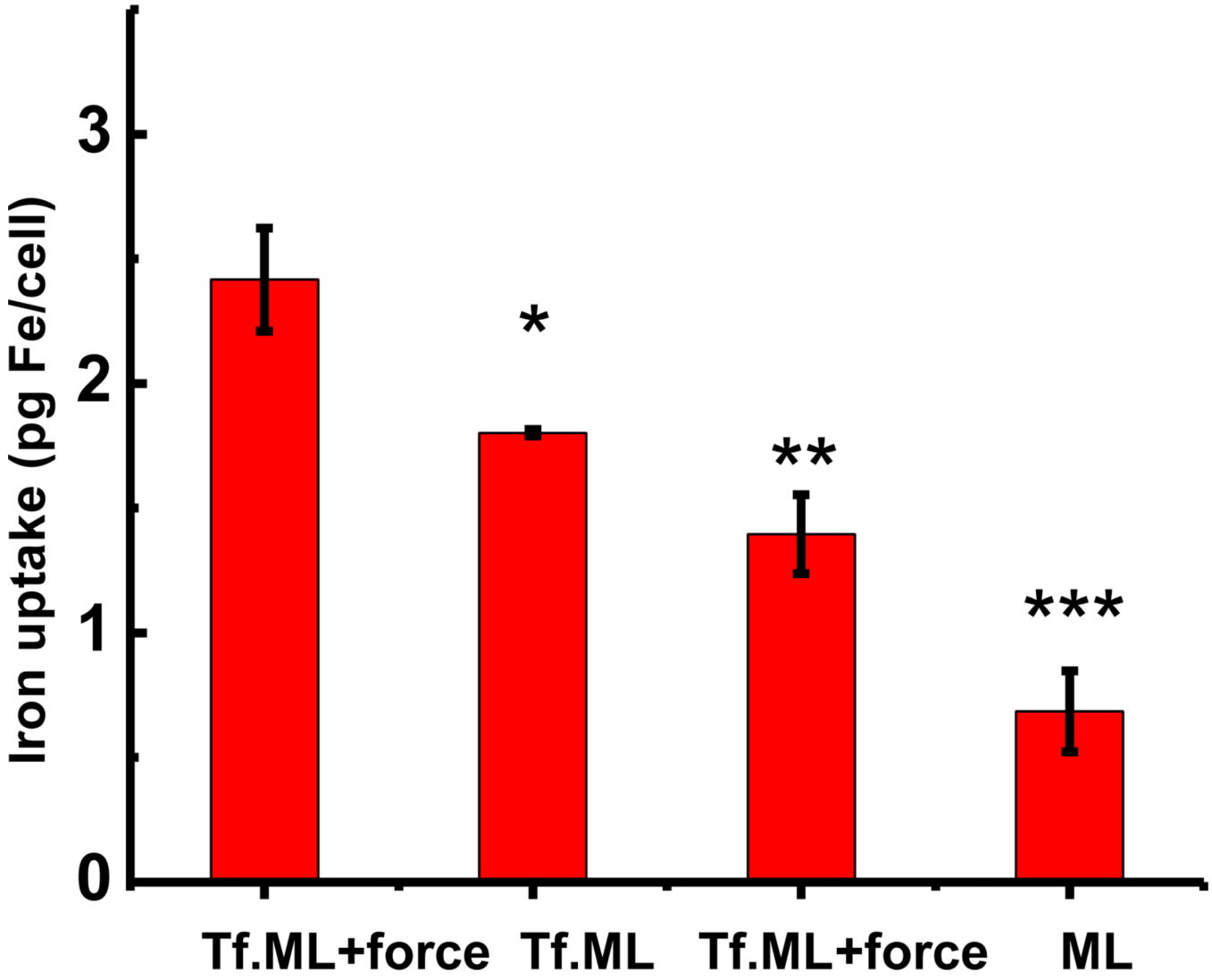

Figure 8.

The Fe_3O_4 content in BBB cells exposed to Transferrin embedded and non-embedded ML nanocarriers in the presence and absence of external magnetic force. Fe_3O_4 uptake due to synergic effect of Transferrin and external magnetic force (Tf.ML+force) were compared to that due to Transferrin (Tf.ML), magnetic force (ML+Force) or lacking both (ML) and P values were calculated. (*p=0.0227; **p=0.0029; ***p=0.0017; Tf: Transferrin; ML: magnetic nanoparticles liposome; Force: external magnetic force).

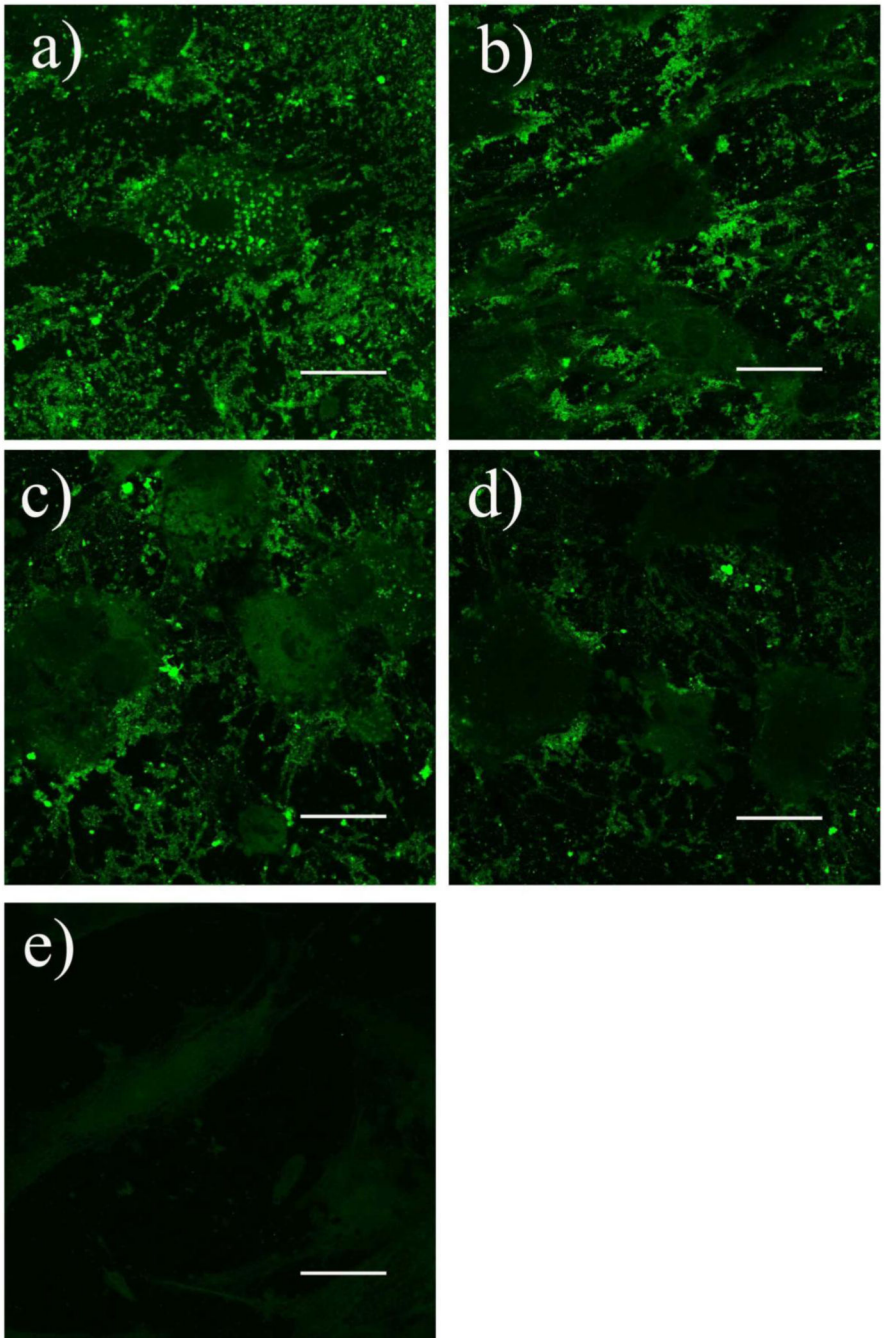

Figure 9.

Confocal microscopy: Synergy effect of Transferrin and external magnetic force (Tf.ML +force) (a) resulted in highest and more uniform MLPs-based luminescence pattern in endothelial cells comparing to ML nanocarriers having only magnetic force (ML+Force) (b), Transferrin (Tf.ML) (c) or lacking both (ML) (d). Fluorescence was absent from untreated cells (e). Scale bar = 20 μm.

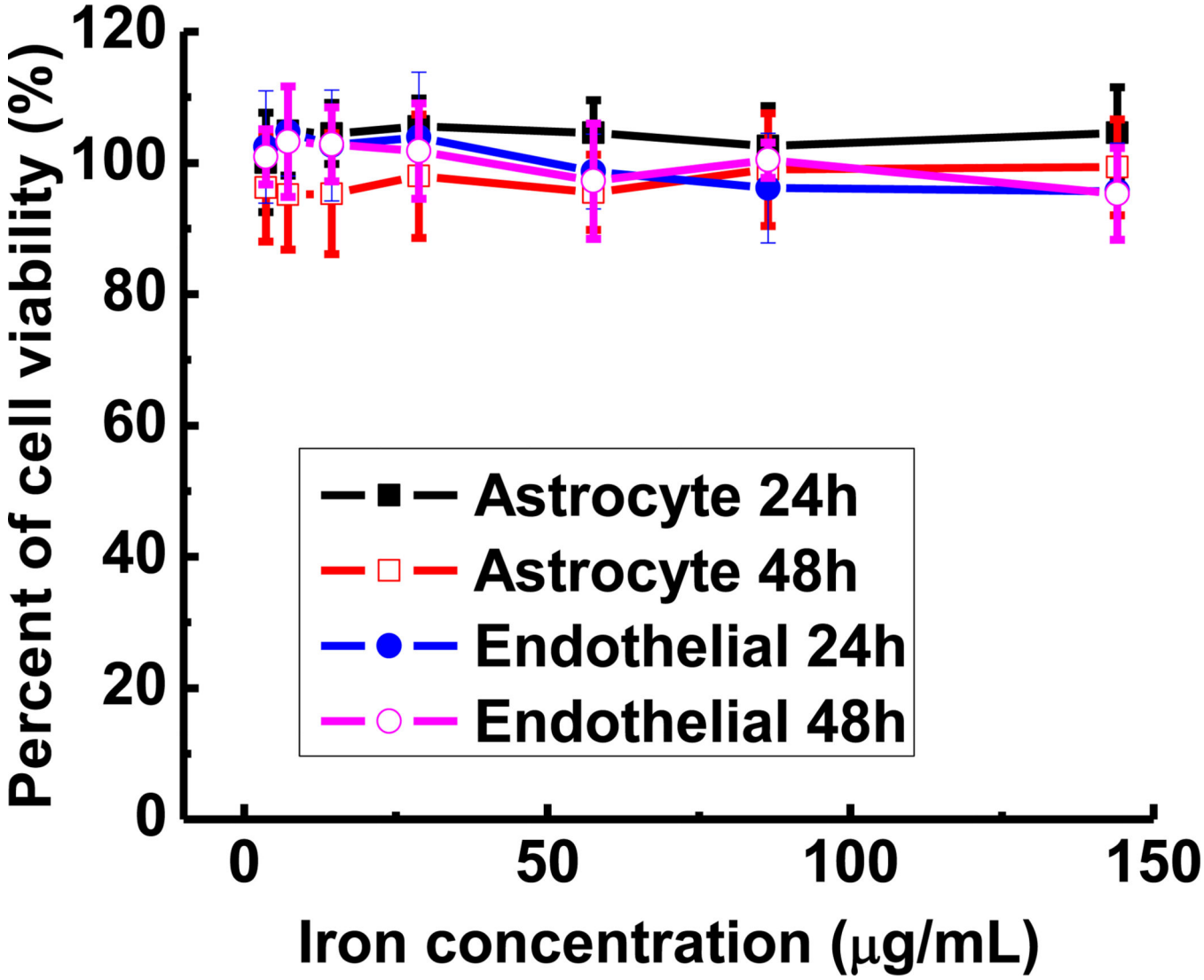

Figure 10.

Percent cell viability of primary endothelial cells and astrocyte cells 24 and 48 hrs post-treatment with different concentration of ML nanocarriers.

Table 1

Transendothelial electrical resistance (TEER) values of the in vitro BBB model before and after treatment of transferrin embedded and non-embedded ML nanocarriers in the presence and absence of external magnetic force.

TEER values (ohms/cm^2)	Tf.ML + Force	ML + Force	Tf. ML	ML	Untreated
Before treatment	189.5±7.5	190.2±6.8	189.6±8.8	191.2±8.5	192.2±9.5
After treatment	186.2±8.1	188.2±8.1	187.8±7.7	187.8±8.4	190.6±8.9

(Tf: Transferrin; ML: magnetic nanoparticles liposome; Force: external magnetic force.)